DOI: 10.64302/joshusc.v32n1c.1323

NUMERICAL ANALYSIS OF DISPERSION CHARACTERISTICS OF TELLURITE-BASED TWPN/I/6 PHOTONIC CRYSTAL FIBER

Hoang Trong Duc, Nguyen Thi Thuy*

University of Education, Hue University

* Email: nguyenthithuy@dhsphue.edu.vn; ntthuy@hueuni.edu.vn

Received: 13/11/2025; Received in revised form: 19/11/2025; Accepted: 21/12/2025

ABSTRACT

In this work, we propose and numerically analyze the large-core tellurite glass (TWPN/I/6) photonic crystal fibers with an octagonal cladding structure. The wavelength-dependent effective refractive index and dispersion are investigated over the 1.0–6.0 μm spectral range. The results show that the maximum and minimum effective refractive indices are 2.051 and 2.005, corresponding to structures with Λ = 1.5 μm; d/Λ = 0.3 and Λ = 0.875 μm; d/Λ = 0.7, respectively. Furthermore, two optimized fibers (Λ = 0.875 μm; d/Λ = 0.3 and Λ = 1.0 μm; d/Λ = 0.3), exhibit flat dispersion profile with low values at suitable pump wavelengths, confirming their potential application in mid-infrared supercontinuum generation.

Keywords: Octagonal cladding, Photonic crystal fibers, flat dispersion, supercontinuum generation.

I. INTRODUCTION

Photonic crystal fiber (PCF) is a new generation of optical fiber with a unique geometric structure, distinct from conventional optical fibers that rely on the refractive index difference between the core and cladding regions. PCFs are designed with a periodic array of air holes running along the fiber length, enabling flexible and precise control of the guiding mechanism. Owing to this structure, PCFs exhibit several remarkable advantages, such as endlessly single-mode operation, tailorable dispersion characteristics, the ability to realize either large mode areas or highly confined modes, as well as enhanced nonlinear effects [1]. Consequently, PCFs have become an ideal platform for supercontinuum generation (SCG), in which a narrowband laser pulse propagating through the fiber undergoes various nonlinear and dispersive processes,

leading to a dramatic spectral broadening and the formation of a broadband, continuous light source. The mechanism of supercontinuum formation can be effectively controlled through the engineered dispersion characteristics of PCFs, achieved by tailoring the air-hole geometry and material composition. As a result, optimized performance with a spectral coverage extending from the visible to the infrared region can be obtained, making PCFs highly suitable for a wide range of photonic applications [2].

Silica-based PCFs have demonstrated many outstanding advantages in SCG applications due to their low cost and transparency window covering the visible and near-infrared regions. However, generating SCG in the mid-infrared (mid-IR) region is challenging because of the very high optical loss at wavelengths beyond 2.0 μm [3-5]. Consequently, tellurite glass has emerged as a highly promising material platform for mid-IR photonics, as its nonlinear refractive index is one to two orders of magnitude higher than that of silica, and its optical transparency window extends up to 5.5 μm in the infrared region [6, 7]. These characteristics make tellurite-PCFs ideal for applications in SCG, pulse compression, coherence tomography, and spectroscopy meteorology [8-10].

Numerous experimental investigations and numerical simulations have demonstrated the potential of tellurite-based PCFs for efficient SCG [6,7,11,12]. Various geometrical designs have been optimized to achieve both anomalous and all-normal dispersion, with the zero-dispersion wavelength (ZDW) shifted into regions favorable for broadband SCG. Solid-core PCFs and hexa-spiral twisted structures exhibit extremely large nonlinearities and well-tailored dispersion, with the ZDW effectively tuned near 1650 nm [6]. In addition, tellurite PCFs with a hexagonal lattice, in which the air holes of the four inner rings surrounding the core are reduced in size, provide a very flat all-normal dispersion profile of approximately –10 to –50 ps/(nm·km) across the 1500–2400 nm range [13]. More recently, octagonal lattice geometries and large-core $Ga_8Sb_{32}S_{60}$ have been explored to combine low confinement loss with high nonlinearity. These designs offer additional degrees of freedom in tailoring the dispersion landscape, enabling simultaneous optimization of the ZDW position, flattened dispersion, and enhanced mode-field control, which are highly beneficial for stable and broadband SCG [14].

In this work, to the best of our knowledge, we propose for the first time a tellurite-based TWPN/I/6 photonic crystal fiber that combines an octagonal cladding lattice with a large-core design created by completely removing the first ring of air holes surrounding the core. This design supports both all-normal and anomalous dispersion regimes over a broad wavelength range from 1.0 to 6.0 μm, with the ZDW shifting toward shorter wavelengths as the filling factor (d/Λ) and lattice constant (Λ) are varied. Based on dispersion analysis, we further present two optimized PCF

structures that exhibit flat dispersion profiles with very low values of –4.188 and 2.148 ps/(nm·km) at pump wavelengths of 2.25 and 1.95 μm, respectively, making them highly suitable for broadband, coherent SCG in the mid-IR region.

II. NUMERICAL MODELING OF THE PCFs

The Lumerical MODE Solutions software was employed to model the structure of the tellurite TWPN/I/6 photonic crystal fibers (T-PCFs). The tellurite glass, denoted as TWPN/I/6 and synthesized within the oxide system $65TeO_2–28WO_3–5Na_2O–2Nb_2O_5$ [mol%], was incorporated into the material database using the Sellmeier coefficients of its linear refractive index, as given by Eq. (1) [13]. As shown in Fig. 1, the refractive index of TWPN/I/6 tellurite glass decreases monotonically with increasing wavelength in the 1.0–6.0 μm range. This trend reflects the intrinsic normal material dispersion of tellurite glass, which dominates in the near-infrared and mid-infrared regions. Such a dispersion characteristic provides a favorable basis for photonic crystal fiber design, where the geometrical contribution can be engineered to counterbalance the material dispersion, enabling the realization of both all-normal and anomalous dispersion regimes for broadband SCG applications.

$$n=\sqrt{1+\frac{2.49628\lambda^2}{\lambda^2-0.01699}+\frac{0.79831\lambda^2}{\lambda^2-0.07728}+\frac{1.8848\lambda^2}{\lambda^2-162.9949}} \quad (1).$$

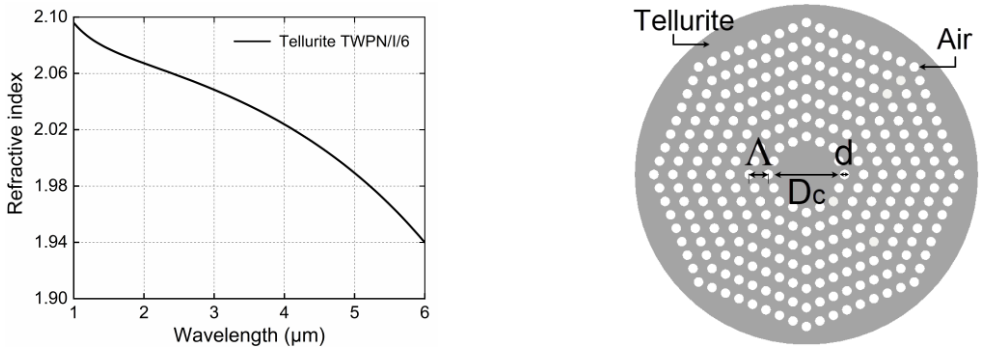

(a) (b)

Fig. 1. The wavelength-dependent refractive indexs of tellurite TWPN/I/6 are extrapolated using Sellmeier's equation [13] (a) and the cross section of the T-PCF.

The T-PCF structures are modeled with an octagonal cladding consisting of seven concentric air-hole rings periodically arranged along the core axis. In solid-core PCFs, the core size together with the nearest air-hole rings strongly governs the dispersion properties, including flatness over a broad wavelength range, slope, value at the pump wavelength, and the ZDW shift. The outer air-hole rings, in contrast, mainly influence the nonlinear characteristics, particularly the confinement loss of the fundamental and higher-order modes [15, 16]. Following this concept, a large solid

core is realized by removing the first ring of air holes surrounding the core, resulting in a core diameter of Dc = 4Λ – d. To investigate the effective refractive index and dispersion properties, the filling factor d/Λ varies between 0.3 and 0.7, while the lattice constant Λ takes the values of 0.875, 1.0, 1.25, and 1.5 μm. A two-dimensional view of the T-PCF structure is shown in Fig. 1(b).

The optical properties, including the effective refractive index and dispersion, are investigated by numerically solving Maxwell's wave equations (Eq. 2) using the full-vector finite-difference eigenmode FDE method for light propagation in the T-PCFs. Perfectly matched layer PML absorbing boundaries are applied to emulate an open domain, thereby suppressing radiation outside the computational window and preventing spurious reflections at the edges.

$$\frac{\partial^2 E(r,\omega)}{\partial z^2} + k\left(\omega^2\right)E(r,\omega) = \Delta_\perp E(r,\omega) - \mu_0\omega^2 P_{NL}(r,\omega) \quad (2),$$

$$E(r,\omega) = \int_{-\infty}^{\infty} E(r,t)\,dt, r = \{x,y,z\} \quad (3),$$

where $E(r,t)$ is the field propagating along z direction, $E(r,\omega)$ denotes the Fourier transform of $E(r,t)$. $P_{NL}(r,\omega)$ and $k(\omega) = n(\omega)\omega/c$ are the Fourier transform of the nonlinear polarization and wave number, respectively.

III. RESULTS AND DISCUSSION

Fig. 2 presents the wavelength dependence of the real part of the effective index, Re[n_{eff}], for T-PCFs with different lattice constants Λ (0.875–1.5 μm) and filling factors d/Λ (0.3–0.7). In all cases, Re[n_{eff}] decreases monotonically with λ, consistent with normal dispersion in solid-core PCFs. For fixed Λ, larger d/Λ lowers Re[n_{eff}] due to stronger air filling and weaker modal confinement; e.g., at Λ = 1.0 μm and λ = 1.55 μm, Re[n_{eff}] decreases from 2.05 (d/Λ = 0.3) to 1.92 (d/Λ = 0.7). For fixed d/Λ, increasing Λ increases Re[n_{eff}] across the spectrum, reflecting stronger core guidance; e.g., at d/Λ = 0.5 and λ = 2.0 μm, Re[n_{eff}] rises from 2.014 (Λ = 0.875 μm) to 2.048 (Λ = 1.5 μm).

At λ = 2.0 μm, Tab.1 shows Re[n_{eff}] ranges narrowly from 2.005 (Λ = 0.875 μm, d/Λ = 0.70) to 2.051 (Λ = 1.5 μm, d/Λ = 0.30). Physically, a higher Re[n_{eff}] corresponds to stronger confinement and reduced leakage, while a lower Re[n_{eff}] enhances the index contrast and increases the waveguide dispersion contribution. Consequently, larger d/Λ and smaller Λ yield stronger negative waveguide dispersion, shifting the ZDW toward shorter wavelength and facilitating access to anomalous dispersion. In contrast, smaller d/Λ and larger Λ flatten dispersion and shift the ZDW to longer wavelength region, which is advantageous for achieving stable all-normal dispersion regimes.

Overall, these results demonstrate that both the lattice constant Λ and the filling factor d/Λ provide effective means of engineering the effective index of T-PCFs. These effective-index trends directly impact waveguide dispersion: higher d/Λ and smaller Λ lead to a stronger negative waveguide contribution, shifting the ZDW toward shorter wavelengths range and enabling anomalous dispersion regimes. Conversely, smaller d/Λ and larger Λ reduce the waveguide contribution, favor flatter all-normal dispersion, and shift the ZDW toward longer wavelengths or even beyond the spectral window of interest.

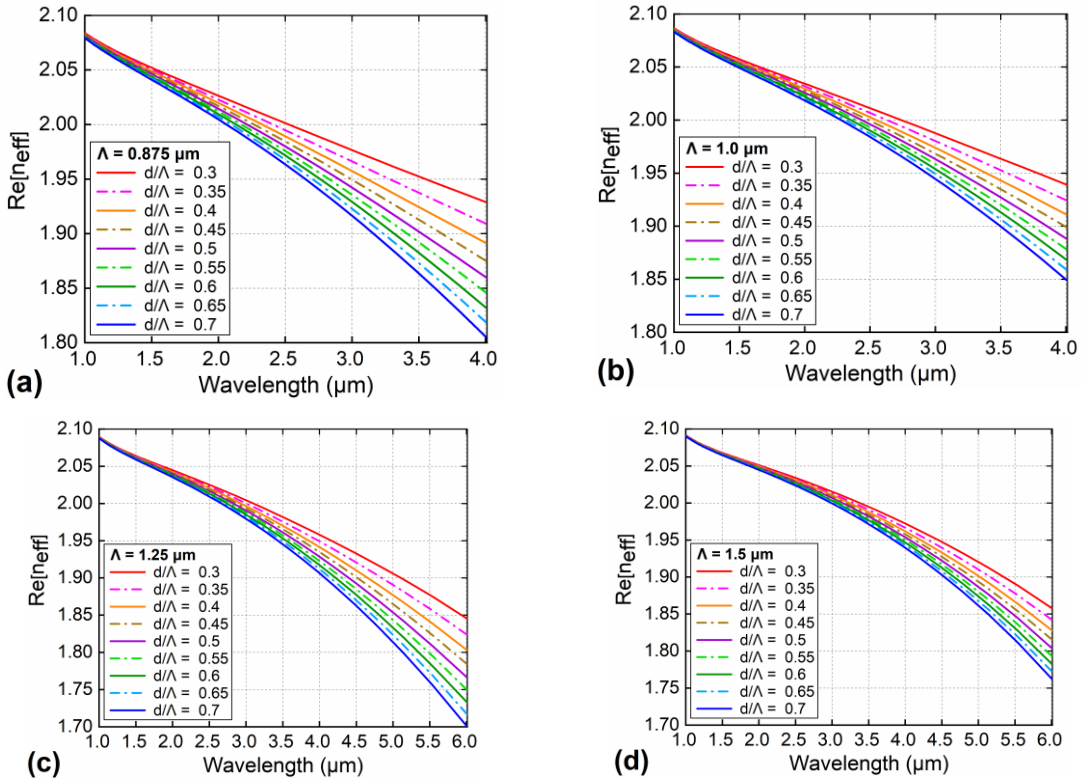

Fig. 2. The real part of effective refractive index of T-PCFs is a function of wavelength with different values of d/Λ and Λ = 0.875; 1.0; 1.25, and 2.0 μm

Tab. 1. The real part of the effective refractive index at 2.0 μm with different values of d/Λ and Λ

Re[n_{eff}]				
d/Λ	Λ = 0.875 μm	Λ = 1.0 μm	Λ = 1.25 μm	Λ = 1.5 μm
0.3	2.026	2.034	2.045	2.051
0.35	2.023	2.032	2.043	2.05
0.4	2.02	2.03	2.042	2.049
0.45	2.017	2.028	2.041	2.049
0.5	2.014	2.026	2.04	2.048

0.55	2.012	2.024	2.039	2.047
0.6	2.01	2.022	2.038	2.046
0.65	2.007	2.02	2.036	2.045
0.7	2.005	2.018	2.035	2.045

During the SCG process, the output spectral characteristics including bandwidth and coherence, are strongly influenced by the dispersion regime, whether it is entirely normal or anomalous. These regimes are associated with two distinct femtosecond pulse pumping mechanisms. To achieve an ultra-broadband SCG, PCFs are typically pumped in the anomalous dispersion regime. In this case, dispersive waves (DW) and soliton dynamics such as soliton fission (SF), stimulated Raman scattering (SRS), and soliton self-frequency shift (SSFS), govern the formation and evolution of the SCG spectrum. However, the coherence of the SCG in this regime is often low due to its sensitivity to noise amplification, resulting in spectral structures with significant fluctuations. In contrast, SCG generated under the all-normal dispersion regime can preserve the temporal integrity of optical pulses and significantly suppress noise. Two dominant nonlinear effects, self-phase modulation (SPM) at the initial stage followed by optical wave breaking (OWB), play key roles in spectral broadening, although the resulting bandwidth is typically narrower [1].

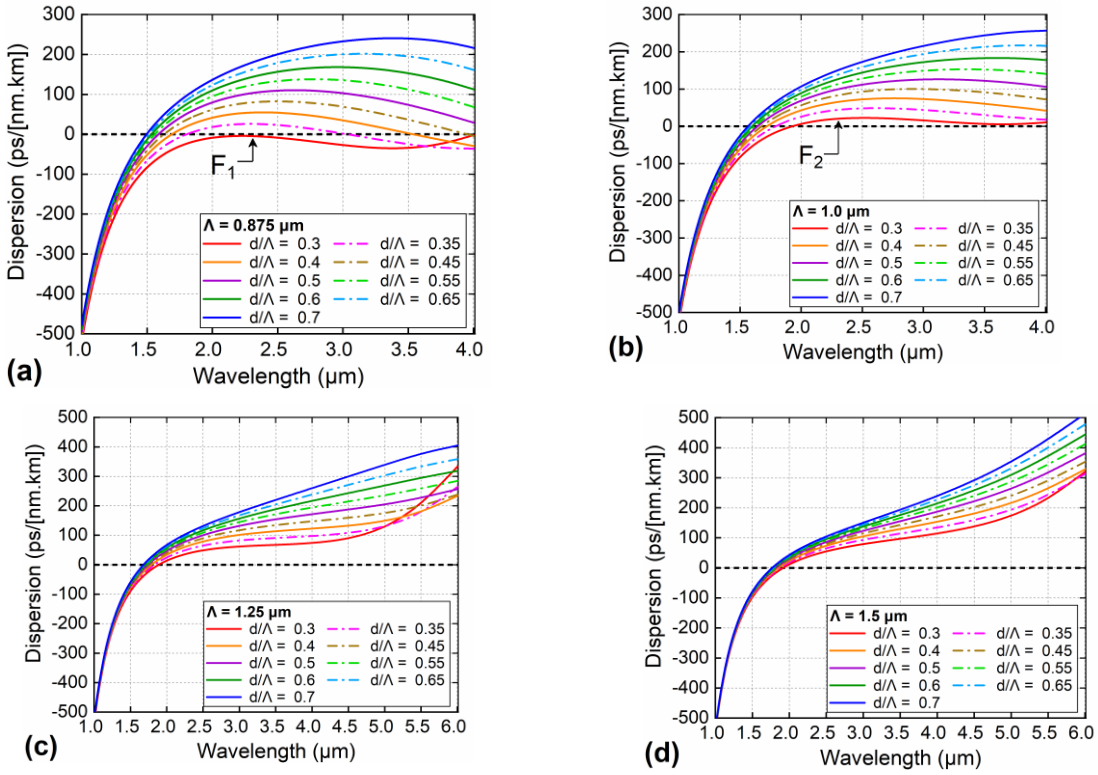

Fig. 3. The dispersion properties of T-PCFs is a function of wavelength with different values of d/Λ and Λ = 0.875; 1.0; 1.25, and 2.0 μm

The total dispersion, $D(\lambda)$, arises from two contributions: the material dispersion, $D_m(\lambda)$, originating from the wavelength-dependent refractive index of the fiber material, and the waveguide dispersion, $D_w(\lambda)$, resulting from the wavelength dependence of the mode propagation constant. While material dispersion is intrinsic to the fiber material and does not depend on the fiber geometry, waveguide dispersion is determined by the fiber structure and its geometrical parameters. Accordingly, the overall dispersion $D(\lambda)$ can be expressed as [1]:

$$D(\lambda) = -\frac{\lambda}{c}\frac{d^2\left(\mathrm{Re}\left[n_{\mathrm{eff}}\right]\right)}{d\lambda^2} \qquad (4),$$

with $\mathrm{Re}[n_{\mathrm{eff}}]$ is the real part of the effective index of the propagating mode in the O-PCF.

The dispersion properties of the proposed T-PCFs are presented in Fig. 3, showing their strong dependence on the d/Λ and Λ. An all-normal dispersion profile is observed only for the smallest d/Λ = 0.3 with a lattice constant of 0.875 μm. As either the d/Λ or Λ increases, the dispersion shifts entirely into the anomalous regime across the wavelength range. This transition from normal to anomalous dispersion is consistent with the corresponding variation of the real part of the effective refractive index, $\mathrm{Re}[n_{\mathrm{eff}}]$, confirming the close relationship between structural parameters and mode properties. Smaller d/Λ values favor extended regions of normal dispersion, while larger d/Λ and Λ enhance mode confinement, resulting in anomalous behavior. In summary, these results demonstrate a clear trend in dispersion engineering: all-normal dispersion is achievable only under specific low d/Λ conditions, whereas anomalous dispersion dominates otherwise. The consistency with $\mathrm{Re}[n_{\mathrm{eff}}]$ profiles further validates the design approach.

Tab.2. The variation of the ZDWs with different values of d/Λ and Λ

	Λ = 0.875 μm	Λ = 1.0 μm	Λ = 1.25 μm	Λ = 1.5 μm
d/Λ	ZDWs1	ZDWs2	ZDWs1	ZDWs
0.3	D < 0		1.927	1.890
0.35	1.803	3.031	1.791	1.829
0.4	1.69	3.538	1.719	1.789
0.45	1.629	3.952	1.675	1.762
0.5	1.588		1.644	1.740
0.55	1.558		1.62	1.723
0.6	1.535		1.6	1.708

0.65	1.515		1.582	1.693
0.7	1.497		1.566	1.680

Tab. 2 summarizes the variation of the ZDW with respect to the Λ and the d/Λ. It is observed that for a fixed Λ, increasing d/Λ results in a continuous blue-shift of the ZDW, attributed to the enhanced waveguide dispersion due to stronger index contrast. Conversely, for a fixed filling factor, enlarging Λ induces a red-shift of the ZDW, as the waveguide contribution becomes weaker compared to the material dispersion. Interestingly, in the case of Λ = 0.875 μm with d/Λ = 0.35–0.45, two ZDWs are obtained, indicating the formation of an anomalous dispersion window sandwiched between two normal dispersion regimes. This feature is advantageous for supercontinuum generation and soliton dynamics.

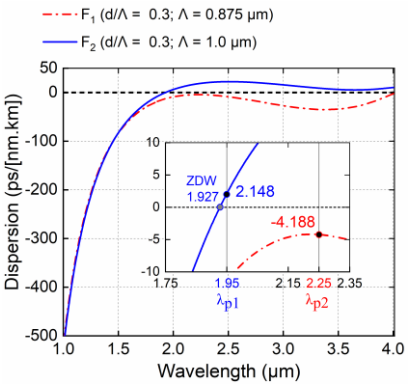

Fig.4. The dispersion properties of two optimal T-PCFs

From the dispersion analysis, two optimal T-PCFs are proposed with dispersion profiles tailored SCG either in the all-normal or in the anomalous regime (Fig. 4). For design F_1 (Λ = 0.875 μm, d/Λ = 0.30), the pump wavelength was chosen at 2.25 μm, corresponding to a local maximum of the dispersion curve. At this point, the dispersion value is relatively low (–4.188 ps/(nm·km)) (Tab. 3), which favors efficient spectral broadening. Pumping here ensures that SCG occurs entirely in the normal-dispersion regime, dominated by SPM and FWM, leading to a smooth and coherent spectrum. This makes F_1 an excellent candidate for stable all-normal-dispersion SC sources in the mid-IR. For design F_2 (Λ = 1.0 μm, d/Λ = 0.30), the pump wavelength is set at 1.95 μm, slightly above the zero-dispersion wavelength (ZDW = 1.927 μm). At this wavelength, the dispersion is relatively low (D = 2.148 ps/(nm·km)) (Tab. 3), ensuring a favorable balance between dispersion and nonlinearity. Pumping in this anomalous regime allows the excitation of higher-order solitons and subsequent fission, while the close proximity to ZDW enhances dispersive-wave generation. This combination leads to a broader and more asymmetric supercontinuum compared to

the all-normal dispersion case. Therefore, F_2 is well suited for soliton-driven SCG with extended bandwidth in the mid-IR.

Tab.3. The structural parameters and characteristic values of two optimal T-PCFs

#	D_c	Λ	d/Λ	Pump wavelength	Re[n_{eff}]	D
	(μm)	(μm)		(μm)		ps/(nm·km)
F_1	3.238	0.875	0.3	2.25	2.014	–4.188
F_2	3.7	1.0	0.3	1.95	2.037	2.148

In our designs, the optimized dispersion values at the pump wavelengths are relatively small, with −4.188 ps/(nm·km) at 2.25 μm (F_1) and 2.148 ps/(nm·km) at 1.95 μm (F_2). These values are significantly lower than those reported in several previous tellurite PCF studies, where dispersion often exceeded 10–50 ps/(nm·km) in the mid-IR region [13], or dispersion can be kept within 60.47 to 61.33 ps/(nm·km) from 2.15 μm to 2.85 μm wavelength [17]. Conversely, our values are larger than the ultra-flattened dispersion achieved in some telecom PCFs, such as 0.93 and 1.533 ps/(nm·km) over wavelength range from 1.3 to 1.6 μm [18]. The dispersion values obtained in F_1 and F_2 not only facilitate efficient phase matching and enhance nonlinear interactions, but also provide a balanced design trade-off between bandwidth extension and fabrication feasibility.

Nevertheless, The fabrication of Te-based PCFs remains challenging due to thermal and chemical instabilities, but advances in optimized stack-and-draw techniques, extrusion, and protective coatings are essential to enable scalable, low-loss fibers for practical nonlinear photonic applications. Future experimental efforts should focus on composition-tuned tellurite glasses with higher thermal stability, long-length preform fabrication with controlled air-hole uniformity, and integration of large-mode-area or specialty lattice designs to further enhance supercontinuum performance [19].

IV. CONCLUSION

We have systematically analyzed the large-core tellurite (TWPN/I/6) photonic crystal fibers through the effective index and the corresponding dispersion. The octagonal cladding structure and the removal of an inner air-hole ring to form a large core both strongly influence Re[n_{eff}], thereby enabling effective dispersion control. The wavelength dependence of Re[n_{eff}] governs ZDW shifts and allows precise dispersion engineering. Two optimized designs were obtained: F_1 (Λ = 0.875 μm, d/Λ = 0.30) with an all-normal profile and low dispersion of –4.188 ps/(nm·km) at 2.25 μm, and F_2 (Λ = 1.0 μm, d/Λ = 0.30) operating in the anomalous regime with ZDW = 1.927 μm and dispersion of 2.148 ps/(nm·km) at 1.95 μm. These dispersion profiles favor smooth SCG

in the all-normal regime and soliton-driven broadening in the anomalous regime. The results emphasize that octagonal cladding and large-core design enhance the flexibility of Re[n_{eff}]-guided dispersion tuning, providing versatile platforms for mid-IR supercontinuum sources.

REFERENCES

[1]. G. P. Agrawal, Nonlinear Fiber Optics (5th edition), Academic Press, Elsevier 2012. https://doi.org/10.1016/C2011-0-00045-5.

[2]. Dudley, J.M., Taylor, J.R.: Supercontinuum Generation in Optical Fibers. Cambridge University Press (2010). https://doi.org/10.1017/CBO9780511750465.

[3]. Thuy Nguyen Thi, Duc Hoang Trong and Lanh Chu Van, Supercontinuum generation in ultra-flattened near-zero dispersion PCF with C_7H_8 infiltration, Optical and Quantum Electronics 55, 93 (2023). https://doi.org/10.1007/s11082-022-04351-x.

[4]. Thi, T.N., Van, L.C. Supercontinuum spectra above 2700 nm in circular lattice photonic crystal fiber infiltrated chloroform with the low peak power. J Comput Electron (2023). https://doi.org/10.1007/s10825-023-02078-w.

[5]. Thuy Nguyen Thi, Duc Hoang Trong and Lanh Chu Van, Comparison of supercontinuum spectral widths in CCl_4-core PCF with square and circular lattices in the claddings, Laser Phys. 33 (5) (2023) 055102 (13pp). https://doi.org/10.1088/1555-6611/acc240.

[6]. Shaymaa R. Tahhan, Arkadiy Mastin, Izaddeen Kabir Yakasai, Ahmad Atieh, Kawsar Ahme, Francis M. Bui, Fahad Ahmed Al-Zahran, Highly nonlinear tellurite photonic crystal fiber for supercontinuum generation: Design and quantitative performance analysis, Alexandria Engineering Journal 81 (15) (2023). https://doi.org/10.1016/j.aej.2023.09.048.

[7]. Pooja Chauhan, Ajeet Kumar, Yogita Kalra Computational modeling of tellurite based photonic crystal fiber for infrared supercontinuum generation, Optik 187 (2019), pp. 92-97. https://doi.org/10.1016/j.ijleo.2019.03.106.

[8]. Ahmad K. Atieh, Costel Flueraru, Chander Prakash Grover, Extremely flat ultrawideband supercontinuum for WDM/TDM applications, Proceedings Volume 5260, Applications of Photonic Technology 6 (2003). https://doi.org/10.1117/12.543177.

[9]. M. Nisoli; S. De Silvestri; O. Svelto, Generation of high energy 10 fs pulses by a new pulse compression technique, Appl. Phys. Lett. 68, 2793–2795 (1996). https://doi.org/10.1063/1.116609.

[10]. H. Takara, T. Ohara, K. Mori, K. Sato, E. Yamada, Y. Inoue, T. Shibata, M. Abe, T. Morioka, and K. I. Sato, More than 1000 channel optical frequency chain generation from single supercontinuum source with 12.5 GHz channel spacing, Electron. Lett. 36, pp. 2089–2090 (2000). https://doi.org/10.1049/el:20001461.

[11]. Tonglei Cheng, Xiaoyu Chen, Qi Wang, Yuanhongliu Gao, Bin Li, Ning Yang, Xin Yan, Xuenan Zhang, Takenobu Suzuki, Yasutake Ohishi, Zheng Liu, and Fang Wang, Experimental investigation of supercontinuum generation in a birefringence tellurite

microstructured optical fiber, Applied Optics 61(3) pp. 9749-9754 (2022). https://doi.org/10.1364/AO.473596.

[12]. Meisong Liao, Chitrarekha Chaudhari, Guanshi Qin, Xin Yan, Takenobu Suzuki, and Yasutake Ohishi, Tellurite microstructure fibers with small hexagonal core for supercontinuum generation, Optics Express 17 (14), pp. 12174-12182 (2009). https://doi.org/10.1364/OE.17.012174.

[13]. Mariusz Klimczak, Damian Michalik, Grzegorz Stępniewski, Tanvi Karpate, Jarosław Cimek, Xavier Forestier, Rafał kasztelanic, Dariusz Pysz, Ryszard Stępień, and Ryszard Buczyński, Coherent supercontinuum generation in tellurite glass regular lattice photonic crystal fibers, Journal of the Optical Society of America B 36 (2), pp. A112-A124 (2019). https://doi.org/10.1364/JOSAB.36.00A112.

[14]. Thuy Nguyen Thi, Lanh Chu Van, Khanh Nguyen Nhat, Tu Le Tran Uyen, Duc Hoang Trong. Modelling of octagonal $Ga_8Sb_{32}S_{60}$-photonic crystal fiber for LWIR broadband supercontinuum generation. Opt Quant Electron 57, 33 (2025). https://doi.org/10.1007/s11082-024-07920-4.

[15]. T. Nguyen Thi, D. Hoang Trong, L. Chu Van, Broadband supercontinuum generation in different lattices of As_2Se_3-photonic crystal fbers with all-normal dispersion and low peak power, Optical and Quantum Electronics 56:367 (2024). https://doi.org/10.1007/s11082-023-06043-6.

[16]. Lanh Chu Van, Thuy Nguyen Thi, Bao Tran Le Tran, Duc Hoang Trong, Ngoc Vo Thi Minh, Hieu Van Le, Van Thuy Hoang, Multi-octave supercontinuum generation in As2Se3 chalcogenide photonic crystal fiber, Photonics and Nanostructures - Fundamentals and Applications, 48, 100986, (2022). https://doi.org/10.1016/j.photonics.2021.100986.

[17]. Tianye Huang, Pan Huang, Zhuo Cheng, Jianfei Liao, Xu Wu, Jianxing Pan, Design and analysis of a hexagonal tellurite photonic crystal fiber with broadband ultra-flattened dispersion in mid-IR, Optik 167, pp. 144-149 (2018). https://doi.org/10.1016/j.ijleo.2018.04.016.

[18]. Jianfei Liao, Junqiang Sun, Yi Qin, Mingdi Du, Ultra-flattened chromatic dispersion and highly nonlinear photonic crystal fibers with ultralow confinement loss employing hybrid cladding, Optical Fiber Technology 19 (5), pp. 468-475 (2013). https://doi.org/10.1016/j.yofte.2013.05.013.

[19]. E.F. Chillcce, C.M.B. Cordeiro, L.C. Barbosa, C.H. Brito Cruz, Tellurite photonic crystal fiber made by a stack-and-draw technique, Journal of Non-Crystalline Solids 352, pp. 3423–3428 (2006). doi:10.1016/j.jnoncrysol.2006.02.127.

PHÂN TÍCH SỐ TÍNH CHẤT PHÂN TÁN CỦA SỢI TINH THỂ QUANG TỬ TWPN/I/6 GỐC TELLURITE

Hoàng Trọng Đức, Nguyễn Thị Thủy*

Trường Đại học Sư phạm, Đại học Huế

*Email: nguyenthithuy@dhsphue.edu.vn; ntthuy@hueuni.edu.vn

TÓM TẮT

Trong nghiên cứu này, chúng tôi đề xuất và phân tích sợi tinh thể quang tử tellurite (TWPN/I/6) lõi lớn với cấu trúc lớp vỏ dạng bát giác. Chiết suất hiệu dụng và đặc tính tán sắc phụ thuộc bước sóng được khảo sát trong dải 1,0–6,0 μm. Kết quả cho thấy chiết suất hiệu dụng cực đại và cực tiểu lần lượt đạt 2,051 và 2,005, tương ứng với các cấu trúc có Λ = 1,5 μm; d/Λ = 0,3 và Λ = 0,875 μm; d/Λ = 0,7. Ngoài ra, hai cấu hình sợi được tối ưu hóa (Λ = 0,875 μm; d/Λ = 0,3 và Λ = 1,0 μm; d/Λ = 0,3) thể hiện cấu hình phẳng với giá trị tán sắc thấp tại các bước sóng bơm phù hợp, khẳng định tiềm năng ứng dụng của chúng trong việc tạo ra siêu liên tục hồng ngoại giữa.

Từ khóa: lớp vỏ bát giác, sợi tinh thể quang tử, tán sắc phẳng, tạo siêu liên tục.

Hoàng Trọng Đức sinh ngày 06/9/1979 tại Quảng Bình. Ông tốt nghiệp kỹ sư chuyên ngành Kỹ thuật điện năm 2004 tại Trường Đại học Bách khoa, ĐH Đà Nẵng; tốt nghiệp thạc sĩ chuyên ngành Tự động hóa năm 2013 tại trường Đại học Bách khoa, ĐH Đà Nẵng. Ông công tác tại Khoa Vật lí, Trường Đại học Sư phạm, Đại học Huế từ năm 2004.

Lĩnh vực nghiên cứu: Mô phỏng các hiện tượng Vật lí trong vật liệu.

Nguyễn Thị Thủy sinh ngày 02/6/1980 tại Kon Tum. Bà tốt nghiệp cử nhân ngành Sư phạm Vật lí năm 2002 tại Trường Đại học Sư phạm, ĐH Huế; tốt nghiệp thạc sĩ chuyên ngành Vật lí Chất rắn năm 2007 tại Trường Đại học Khoa học, ĐH Huế, nhận học vị tiến sĩ năm 2015 tại Trường Đại học Khoa học Tự nhiên, ĐH Quốc gia Hà Nội; được công nhận Phó Giáo sư năm 2024. Bà công tác tại Khoa Vật lí, Trường Đại học Sư phạm, ĐH Huế từ năm 2002.

Lĩnh vực nghiên cứu: Quang học.